Molecular Therapy
Nucleic Acids
Original Article

Synthetic miR-21 decoy circularized by tRNA splicing mechanism inhibited tumorigenesis in glioblastoma *in vitro* and *in vivo* models

Hadi Bayat,[1] Mohammad Hossein Pourgholami,[2] Saeid Rahmani,[3] Safura Pournajaf,[2] and Seyed Javad Mowla[1]

[1]Department of Molecular Genetics, Faculty of Biological Sciences, Tarbiat Modares University, Tehran 14115-111, Iran; [2]Department of Physiology, Faculty of Medical Sciences, Tarbiat Modares University, Tehran 14115-111, Iran; [3]School of Computer Science, Institute for Research in Fundamental Sciences (IPM), Tehran 19538-33511, Iran

Glioblastoma multiforme (GBM) is the deadliest primary central nervous system tumor. miRNAs (miRs), a class of non-coding RNAs, are considered pivotal post-transcriptional regulators of cell signaling pathways. miR-21 is a reliable oncogene that promotes tumorigenesis of cancer cells. We first performed an *in silico* analysis on 10 microarray datasets retrieved from TCGA and GEO databases to elucidate top differentially expressed miRs. Furthermore, we generated a circular miR-21 decoy, CM21D, using the tRNA-splicing mechanism in GBM cell models, U87 and C6. The inhibitory efficacy of CM21D with that of a linear form, LM21D, was compared under *in vitro* conditions and an intracranial C6 rat glioblastoma model. miR-21 significantly overexpressed in GBM samples and confirmed in GBM cell models using qRT-PCR. CM21D was more efficient than LM21D at inducing apoptosis, inhibiting cell proliferation and migration, and interrupting the cell cycle by restoring the expression of miR-21 target genes at RNA and protein levels. Moreover, CM21D suppressed tumor growth more effectively than LM21D in the C6-rat GBM model ($p < 0.001$). Our findings validate miR-21 as a promising therapeutic target for GBM. The introduced CM21D by sponging miR-21 reduced tumorigenesis of GBM and can be considered a potential RNA-base therapy to inhibit cancers.

INTRODUCTION

Glioblastoma multiforme (GBM; grade IV) is the deadliest and most treatment-resistant primary central nervous system tumor, accounting for approximately 50% of all gliomas with a high recurrence rate and dismal overall survival of less than 8.5 months. GBM emanates from astrocytic glial cells, and its incidence is estimated at approximately 4.17 per 100,000 person-years.[1] Surgical resection combined with chemotherapy and radiotherapy is the first-line therapeutic approach for GBM. However, because of the infiltrative nature and intra- and inter-tumoral genetic heterogeneity of GBM, the current standard management of surgery combined with radiotherapy and temozolomide has not succeeded.[2,3] Therefore, establishing a novel improved targeted therapy of key molecular genetic mediators of GBM is urgent.

According to cumulative reports during recent years, non-coding RNAs (ncRNAs) have emerged as crucial players in cancer. miRNAs (miRs), a class of ncRNAs, are considered pivotal post-transcriptional regulators that directly base pair to their binding sites. This interaction leads to cleavage or translational arrest of target mRNA.[4] miR-21 is an unwavering oncogene upregulated in most cancers, particularly GBM. It has a profound negative influence on critical tumor suppressor genes that prevent tumorigenesis in cancer cells.[5,6] Circular RNAs (circRNAs) are another class of ncRNAs that are covalently closed and mainly generated through the back-splicing mechanism.[7] circRNAs play essential roles in gene expression and can function as a competitive platform for binding gene regulators such as miRs. circRNAs, by sponging miRs, can act as oncogenes or tumor suppressors in cancer cells.[8–11]

Synthetic circRNA decoys or sponges are inspired by naturally occurring ones and applied as potent therapeutic tools in different cancers. Synthetic miR decoys are artificial competitive inhibitors that can induce miR loss-of-function by base pairing through multiple tandem binding sites to target miR.[12] miR decoys can be applied in linear and circular forms and have several advantages over chemically modified antisense oligonucleotides (antagomiRs). First, antagomiRs are limited and can suppress one miR because their efficient binding depends on complementarity with beyond sequence in addition to the seed region. Second, many cells cannot uptake antagomiRs, and third, antagomiRs must be repeatedly administered in higher doses for extended therapy.[13]

It has recently been shown that *Drosophila* Tyr-tRNA, *CR31905*, splicing mechanism, can process pre-tRNA and extract its intron in a circular form in mammalian cells.[14] By replacing the intron with an RNA-aptamer, this system was used as an *in vitro* and *in vivo* imaging system.[15] Hence, this system can be considered a potent tool for intracellularly generating miR decoys.

In this study, we first performed an *in silico* analysis of 10 microarray datasets retrieved from The Cancer Genome Atlas (TCGA) and Gene

Received 30 December 2022; accepted 4 April 2023;
https://doi.org/10.1016/j.omtn.2023.04.001.

Correspondence: Seyed Javad Mowla, Department of Molecular Genetics, Faculty of Biological Sciences, Tarbiat Modares University, Tehran 14115-111, Iran.
E-mail: sjmowla@modares.ac.ir

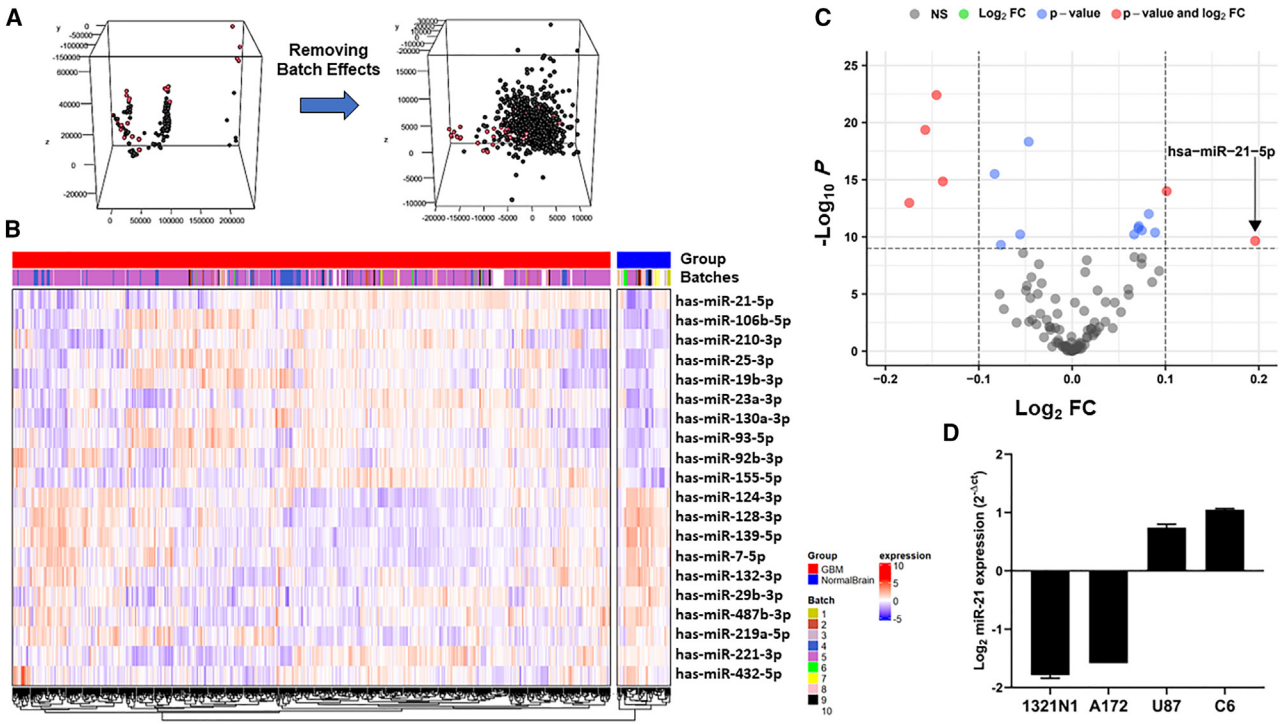

Figure 1. *In silico* analysis of GBM microarray datasets

(A) To perform *in silico* analysis, batch effects between datasets were removed. Normal and GBM samples are indicated with red and black balls, respectively. (B) Limma DEA was applied to the retrieved datasets, and the top miRs-DE were obtained, as shown in the heatmap plot. (C) miR-21 showed the highest fold change expression level. (D) To confirm the *in silico* results, the expression level of miR-21 ($2^{-\Delta ct}$) was measured in GBM cell line models. U87 and C6 cells showed higher relative expression levels and were chosen for further experiments. NS, not significant; FC, fold change.

Expression Omnibus (GEO) databases. We identified miR-21-5p as a reliable oncogene upregulated in GBM tumor cells. Moreover, we designed a circular miR-21 decoy (CM21D) with three bulged binding sites for miR-21 and compared its inhibitory effects with linear miR-21 decoy (LM21D) in GBM models. We used a tRNA-splicing mechanism to generate circular miR-21decoys. To our knowledge, this is the first application of the tRNA-splicing mechanism to suppress miR-21 expression in an experimental model of GBM, employing both *in vitro* and *in vivo* procedures. Furthermore, to ensure that the *in vitro* results translate to an *in vivo* effect, CM21D and LM21D were evaluated in an intracranial C6 rat model.

RESULTS

Identification of noteworthy differential expressed miRs and coding genes in GBM

Publicly available GBM microarray datasets from the TCGA and GEO databases were screened. Ten studies were eventually retrieved that focused on small ncRNAs to query differentially expressed (DE) miRs between GBM cases (n = 670) and normal subjects (n = 60) (Figures 1A and S1A, and Table S1). Among the significant miR-DEs (Figure 1B, Table S2), we conducted an additional study with miR-21, widely recognized as a reliable oncogene in various cancers.[16] Based on our results, miR-21 was highly expressed in GBM samples compared with normal subjects (Figures 1C and S1B).

To confirm our *in silico* results, we assessed the expression levels of miR-21 in GBM, 1321N1, A172, U87, and C6 cell lines. Our results showed that miR-21 has a higher expression level in the more invasive GBM cell models, U87 and C6 (Figure 1D).

miR-21 excessively impacted different cellular signaling pathways in most cancer cells (Figure S2). miR-21 inhibits several vital tumor suppressors, such as programmed cell death 4 (PDCD4), reversion-inducing cysteine-rich protein with kazal motifs (RECK),[17] tissue inhibitor of metalloproteinases 3 (TIMP3),[18] and phosphatase and tensin homolog (PTEN),[19] and has a positive correlation with over-expression of matrix metalloproteinases (MMPs),[20] vascular endothelial growth factor A (VEGFA),[21] and B-cell lymphoma 2 (BCL2) apoptosis regulator.[22] Here, we analyzed the available microarray datasets in the TCGA database to elucidate the positive and negative correlations between miR-21 and the candidate coding genes. As presented in the heatmap graph, oncogenic proteins were positively correlated, while tumor suppressors were negatively correlated with miR-21 (Figure S2C).

Designing miR-21 sponge

Our previous study found that a synthetic linear decoy with three perfect complementary binding sites for miR-21 could reduce tumor volume in the GBM rat model.[17] Linear RNA decoys are susceptible to

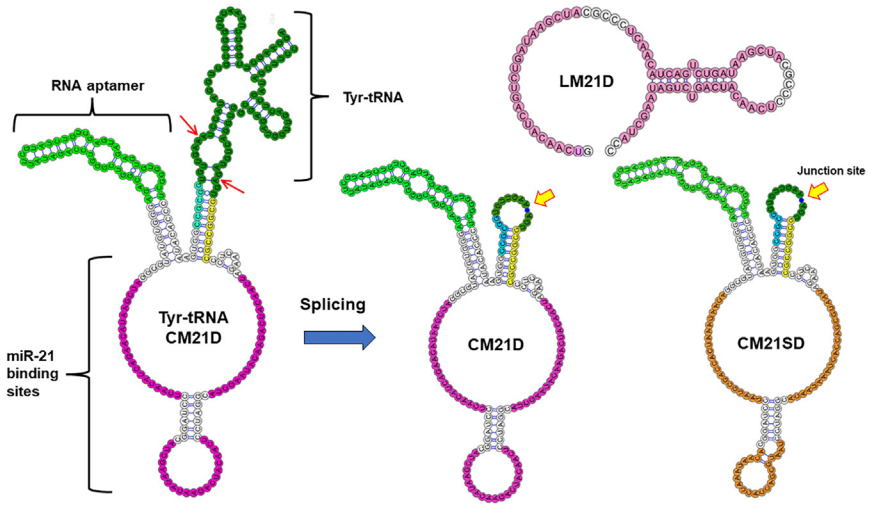

Figure 2. Schematic representation of circular miR-21 decoys generation using a tRNA-splicing mechanism and LM21D

The secondary structure of the *Drosophila* Tyr-tRNA-CM21D, CM21D, CM21SD, and LM21D was predicted by MXfold2 and visualized using VARNA v3.93 (RRID: SCR_006459). tRNA (dark green), miR-21 bulged binding site (purple), miR-21 perfect binding site (light purple), miR-21 scrambled binding sites (orange), and RNA aptamer (light green). Red arrows indicate splice sites in Tyr-tRNA CM21D. The NotI (yellow) and SacII (light blue) restriction sites can be used to replace CM21D with CM21SD. Yellow arrows indicated the junction sites on CM21D and CM21SD.

RNase degradation and have short half-lives. Recently, it has been well-documented that bulged circRNA decoys are authoritative tools to seize the oncogenic effects of miRs.[12,23] Therefore, we designed a synthetic circular miR-21 decoy with three bulged binding sites, CM21D, and compared its antitumor impacts with those of the linear form, LM21D. To generate CM21D, we used the *Drosophila* Tyr-tRNA gene, *CR31905*, which splices its intron into a circular shape in mammals.[15] We replaced the intron of this gene with CM21D or scrambled construct, the circular miR-21 scrambled decoy (CM21SD). The secondary structure of the recombinant tRNA gene, CM21D, CM21SD, and LM21D, were predicted by MXfold2 online tool and visualized with VARNA v3.93 software (Figure 2).

RT-PCR confirmed the circularization of CM21D and CM21SD by divergent and convergent primer sets (Figure 3A). The precision of circularization was proved with Sanger sequencing (Figure 3B). To reduce the effect of the vector backbone in subsequent experiments, we subcloned the linear miR-21 decoy into Mock (named LM21D). A map of the vectors designed in this study is presented in Figures S3A–S3E. To assess the generation of miR-21 decoys *in vivo*, their expression levels were measured in the U87 and C6 cell lines. All three constructs were expressed in U87 and C6 cell lines (Figure 3C). To check the stability of these decoys, we measured the expression levels of LM21D and CM21D at different time points. Our results showed that CM21D had a significantly higher expression level 48 h after transfection in U87 and C6 cells (Figure 3D).

An RNA aptamer, Broccoli (49-nt), was embedded in circRNA decoys to validate the expression of CM21D and CM21SD *in vivo* (Figure 2). This RNA aptamer can emit green light in the presence of DFHBI-1T in live cells. The stable cell lines, stU87 and stC6, expressing CM21D showed a GFP-like lumen in the cytoplasm that was not observed in untreated U87 (Figure 4A) and C6 cells (Figure S4). Consistent with these results, CM21D and CM21SD were successfully circularized and expressed in the GBM cell models.

The functional efficiency of CM21D and LM21D using a dual-luciferase assay

We used the TIMP3 3′-untranslated region (UTR), which contains two binding sites for miR-21, and previously showed that it can interact with this miR.[24] To assess the efficiency of CM21D and LM21D, we transfected HEK293-T cells with pTIMP3-UTR, pmiR-21, and the miR-21 decoys in diverse combinations and analyzed Renilla luciferase activity at different time points. Renilla luciferase activity was normalized to the firefly luciferase activity. Overexpression of miR-21 significantly decreased luciferase activity, confirming the accuracy of our experiments. Furthermore, co-transfection of Mock and CM21SD together with pmiR-21 also decreased luciferase activity compared with the control group, ensuring that the Mock and CM21SD did not interact with miR-21. Co-transfection of LM21D or CM21D with pmiR-21 resulted in a significant increase in luciferase activity compared with that in Mock or CM21SD, respectively. CM21D restored luciferase activity more significantly than LM21D did at different time points. Based on this finding, it was concluded that CM21D is more efficient than the linear form (Figure 4B).

CM21D, by sponging miR-21, has a significant impact on cell migration

miR-21 directly targets TIMP3 and RECK as key inhibitors of MMPs and consequently increases cell migration, invasion, and angiogenesis.[4] To confirm the inhibitory effects of CM21D and LM21D, we measured the expression of genes involved in cell migration. In cells expressing CM21D, expression of TIMP3 and RECK was increased, while MMP2 and VEGFA were downregulated more than those expressing LM21D (Figures 4C and 4D). In cell-based experiments, we also observed a significant delay in gap closing in cells expressing CM21D compared with those expressing LM21D in U87 (Figures 5A and 5B) and C6 cells (Figures S5A and S5B). Furthermore, stU87 and stC6 cells expressing the miR-21 decoys showed a significant reduction in cell migration in the transwell assay after 24 h, and CM21D was more efficient than LM21D in U87 (Figures 5C and 5D) and C6 cells (Figures S6A and S6B). The inhibitory effects of miR-21 decoys on genes involved in cell migration were validated at the protein level in stU87 cells. CM21D increased TIMP3 and RECK expression

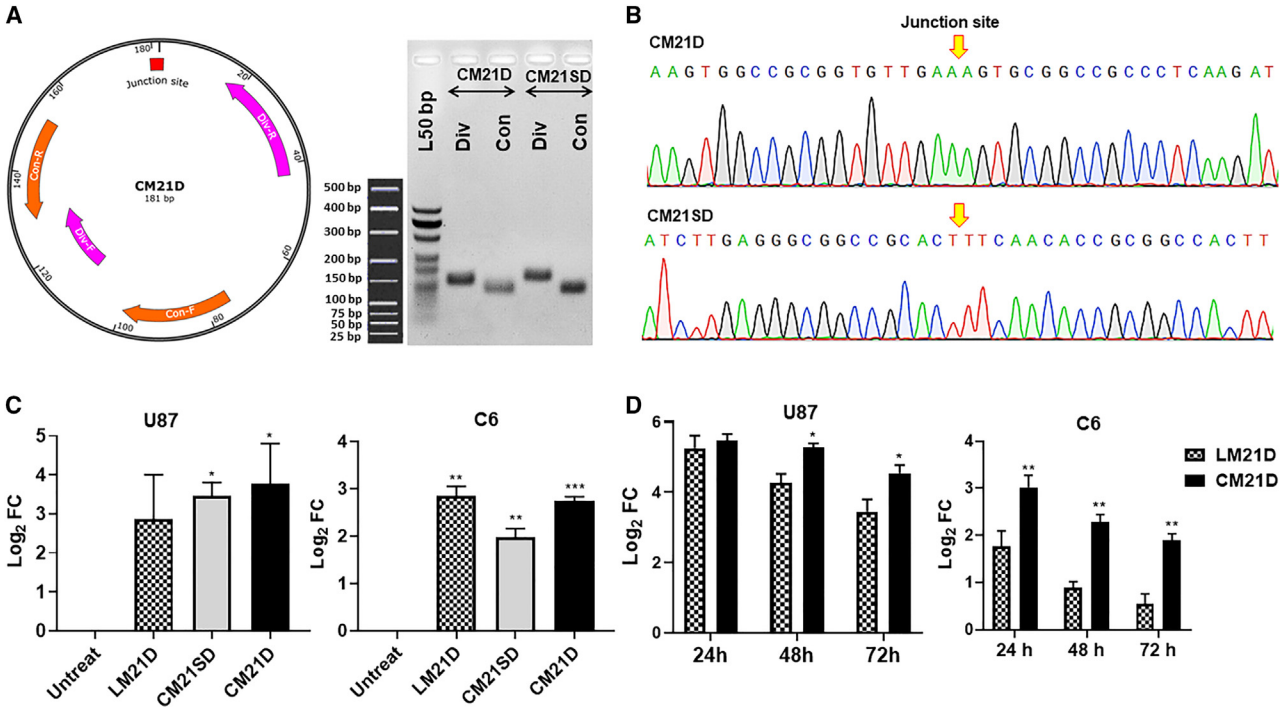

Figure 3. Verifying the circularization and expression of miR-21 decoys

(A) A schematic view of the circularized miR-21 decoys is shown, and the binding sites of the convergent (Con) and divergent (Div) primer sets are indicated. Circularization of CM21D and CM21SD was first confirmed by RT-PCR in stU87 cells (presented) and stC6 cells (data not shown) using Div (113 bp) and Con (78 bp) primer sets on 2% agarose gel. (B) The TA-cloned products of the Div primer set were sequenced by Sanger sequencing, in which yellow arrows indicated junction sites in CM21D and CM21SD. (C) Expression of the miR-21 decoys was measured by qRT-PCR, and all decoys were significantly expressed compared with untreated cells. (D) The stability of LM21D and CM21D was assessed at different time points (24, 48, and 72 h), and CM21D showed a significantly higher expression at different time points in U87 and C6 cell lines ($p < 0.01$ and <0.05, respectively). L50, Ladder 50.

by 2.1- and 1.5-fold, respectively, and decreased MMP2 expression by 0.46-fold (Figure 5E) compared with LM21D. Together, these results demonstrated that CM21D was more efficient at inhibiting cell migration in GBM cells than LM21D.

The inhibition of miR-21 using CM21D significantly decreased cell proliferation

miR-21 targets key tumor suppressors such as PDCD4, heterogeneous nuclear ribonucleoprotein K (HNRNPK), PTEN, TAp63, and SMAD family member 7 (SMAD7), which can promote cell proliferation and enhance the tumorigenesis of cancer cells.[25,26] Our results showed that expression levels of these genes were restored in cells stably expressing CM21D or LM21D were restored. The results for CM21D were more significant than those for LM21D in U87, for example, in the *TAp63* gene ($p < 0.05$) (Figure 6A) and in C6 cells (Figure S7A). To determine the inhibitory effects of the miR-21 decoys on GBM cell models, cell proliferation was estimated using the MTT assay. In the U87 and C6 cell lines, CM21D showed more efficient inhibitory effects than LM21D, especially in U87 cells at 72 h ($p < 0.001$) (Figures 6B and S7B). A CSFE assay was performed to confirm the results of the MTT assay. U87 and C6 cells were stained with CFSE and plated. After 16 h, stained cells were transfected with miR-21 decoys. CM21D caused more excellent growth arrest and accumulation of cell numbers in earlier generations compared with LM21D at 48 h after transfection in U87 (Figures 6C and D) and C6 cells (Figures S7C and S7D). Since circRNA is more stable than the linear form, we performed a soft agar colony formation assay to monitor the inhibitory effect of mmiR-21 decoys over a long period. Our results showed that after 30 days, CM21D significantly reduced colony formation compared to LM21D in U87 ($p < 0.01$) (Figures 6E and 6F) and C6 cells (Figures S7E and S7F). Finally, we analyzed the restoration of gene expression of miR-21 direct target, PDCD4, and HNRNPK, at the protein level. Cells expressing CM21D showed a 3.1- and 1.9-fold increase in PDCD4 and HNRNPK expression compared with LM21D, respectively (Figure 6G). Together, these results demonstrated the greater potency of CM21D in inhibiting GBM cell proliferation.

miR-21 plays a pivotal inhibitory role in apoptosis and cell cycle in GBM cells

Bcl2 associated X-protein (BAX) and BCL2 are critical components of the cellular apoptotic pathway. The increased BAX/BCL2 ratio steered the cells toward apoptosis and vice versa. Hence, in this study, we first analyzed the expression levels of the genes *BAX*, *BCL2*, cyclin-dependent kinase inhibitor 1A (*CDKN1A*), cell division cycle

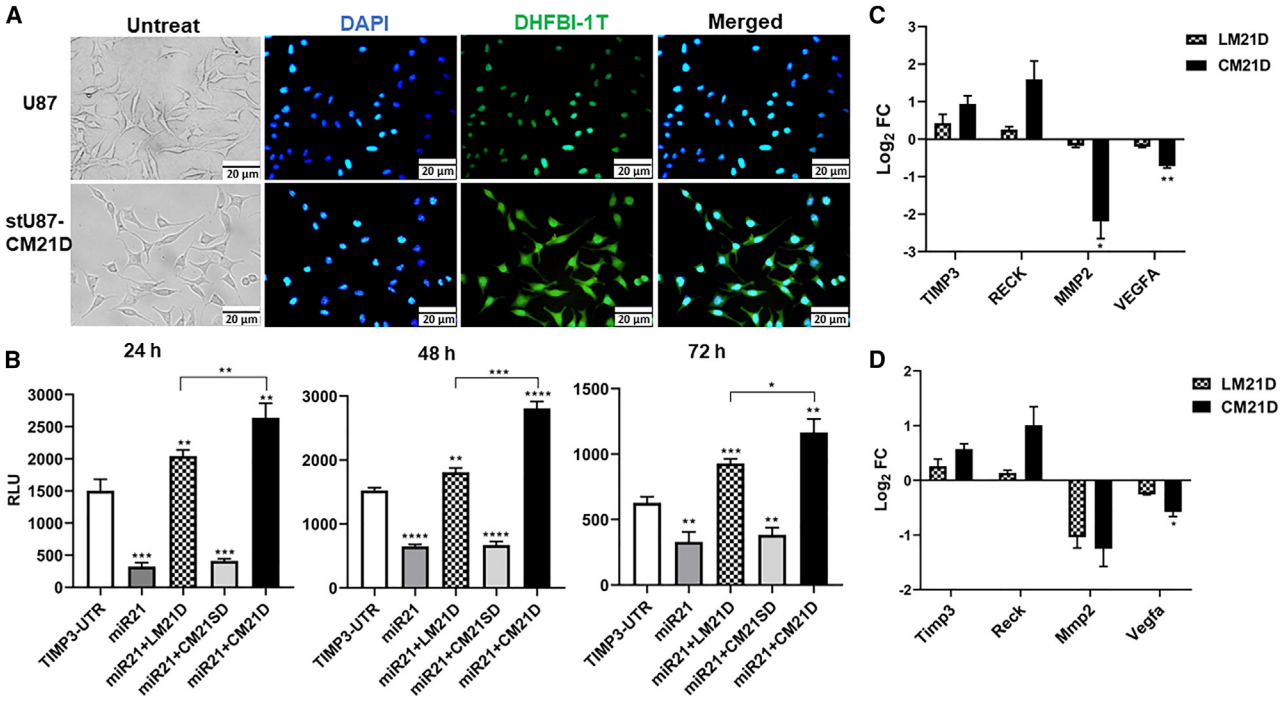

Figure 4. Intracellular expression of CM21D, its interaction with miR-21, and consequent effects on miR-21 target genes

(A) stU87 cells expressing CM21D and U87 cells were stained with DAPI (blue), then DFHBI-1T (green), and merged together, indicating CM21D expression of CM21D in the cell cytoplasm. (B) The interaction of CM21D and LM21D with miR-21 was measured in HEK293T cells at different time points (24 h, 48 h, and 72 h). In all time points, miR-21 significantly decreased the activity of Renilla compared with TIMP3-UTR ($p < 0.001$ at 24 and 48 h; $p < 0.01$ at 72 h). Co-transfection of miR-21 and LM21D increased Renilla activity compared with Mock significantly ($p < 0.01$). In addition, co-transfection of CM21SD and miR-21 decreased the activity of Renilla as miR-21 alone and showed no interaction between miR-21 and CM21SD. Co-transfection of CM21D and miR-21 significantly increased Renilla activity compared with TIMP3-UTR ($p < 0.01$ at 24 and 72 h; $p < 0.001$ at 48 h). CM21D showed higher efficiency than LM21D at different time points ($p < 0.05$ at 24 and 72 h; $p < 0.001$ at 48 h). (C and D) qRT-PCR was performed on U87 and C6 cells expressing LM21D or CM21D. The results were compared with their controls (Mock or CM21SD, respectively). CM21D increased TIMP3 and RECK and decreased MMP2 ($p < 0.05$ in U87) and VEGFA ($p < 0.01$ in U87) more than LM21D in U87 and C6 cells. RLU, relative luciferase unit.

25A (*CDC25A*), and B cell lymphoma/leukemia 11B (*BCL11B*), which are involved in apoptosis and cell cycle, using quantitative RT-PCR (qRT-PCR) in U87 and C6 cells. Cells expressing miR-21 decoys showed increased expression of tumor suppressor genes. Those expressing CM21D showed higher efficiency compared with LM21D (BAX/BCL2 ratio and CDC25A; $p < 0.01$) (Figures 7A and 7B). To elucidate the inhibitory effects of miR-21 decoys, we next estimated apoptosis and the cell cycle status in U87 and C6 cell lines expressing CM21D or LM21D. The apoptosis rate was not significantly altered for LM21D compared with Mock, but CM21D greatly enhanced the apoptosis rate compared with CM21SD and LM21D in U87 cells (Figures 7B and 7C). Moreover, in C6 cells, CM21D significantly decreased the percent of live cells compared with CM21SD ($p < 0.001$) and LM21D ($p < 0.05$). In addition, CM21D significantly increased the apoptosis rates compared with CM21SD ($p < 0.01$). CM21D was more efficient than LM21D in increasing the rate of apoptosis in C6 cells ($p < 0.05$) (Figures S8A and S8B).

Propidium iodide staining of U87 cells expressing either CM21D or LM21D and their controls indicated that CM21D and LM21D significantly increased the sub-G1 population compared with CM21SD and Mock ($p < 0.01$), respectively. Moreover, CM21D was more efficient in increasing sub-G1 cells compared with LM21D ($p < 0.01$) (Figures 7D and 7E). In C6 cells, LM21D and CM21D significantly increased the sub-G1 population compared with Mock ($p < 0.05$) and CM21SD ($p < 0.001$), respectively Figures S9A and S9B). Furthermore, CM21D significantly increases the sub-G1 population more than LM21D in U87 and C6 cells ($p < 0.01$).

Finally, we measured the expression of BAX, BCL2, and CDKN1A at the protein level. Our results showed that LM21D increased the expression of BAX and CDKN1A compared with Mock. Moreover, CM21D remarkably increased the expression of BAX and CDKN1A and decreased BCL2 compared with CM21SD. Compared with LM21D, CM21D increased the amount of the BAX/BCL2 ratio and the expression of CDKN1A by 4.1- and 3.7-fold, respectively (Figure 7F). Consistent with these results, it was concluded that CM21D could reduce the oncogenic effects of miR-21 on apoptosis and the cell cycle more efficiently than LM21D.

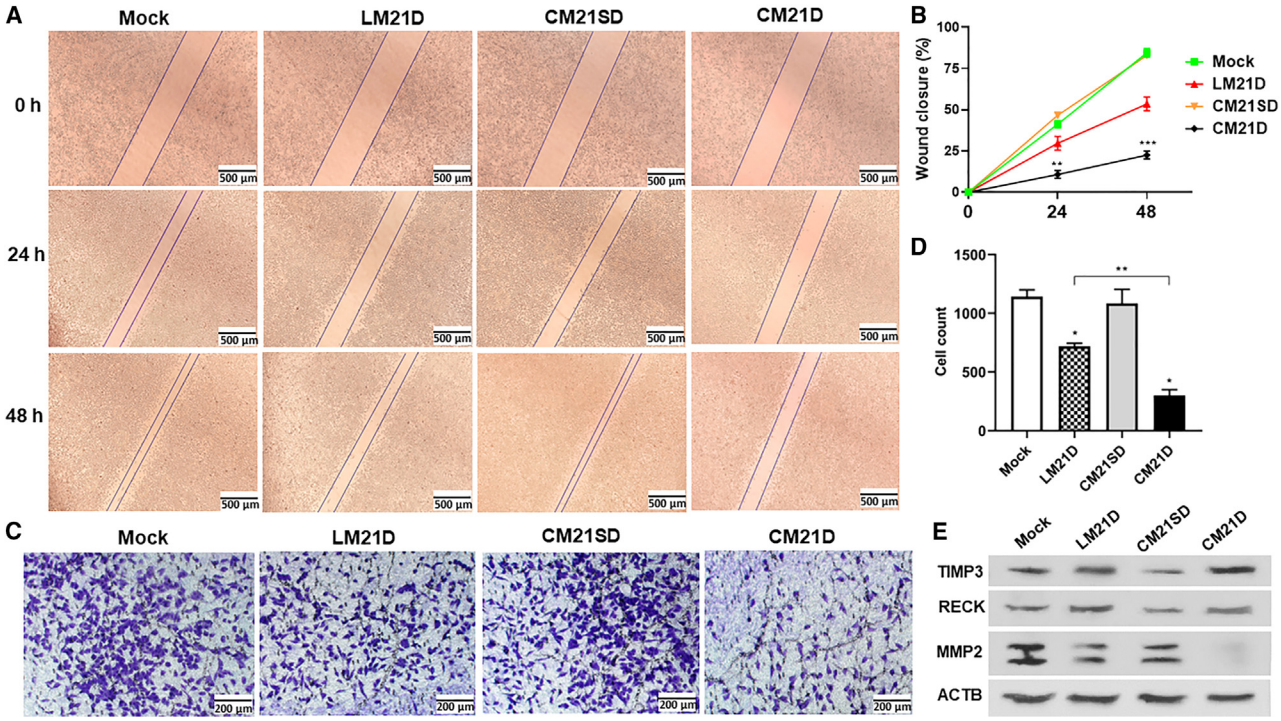

Figure 5. CM21D and LM21D significantly inhibited cell migration

(A and B) The scratch assay was performed on U87 cells, and the gap closure (%) was measured at different time points (0, 24, and 48 h). CM21D more efficiently inhibited U87 cell migration at 24 h ($p < 0.01$) and 48 h ($p < 0.001$) compared with LM21D. (C and D) Transwell assay was performed to analyze cell migration and to confirm scratch assay results. LM21D and CM21D significantly reduced cell migration compared to Mock and CM21SD ($p < 0.05$), respectively. In addition, CM21D significantly decreases cell migration compared with LM21D ($p < 0.01$) in U87 cells. (E) At the protein level, western blotting was performed on TIMP3, RECK, and MMP2. LM21D and CM21D both increased TIMP3 and RECK and decreased MMP2. Moreover, CM21D was more efficient than LM21D.

Antitumor growth effects of designed RNA decoys *in vivo*

To validate the therapeutic potential of CM21D and compare it with that of LM21D, we stereotaxically injected C6 cells stably expressing miR-21 decoys and their controls into the caudate putamen striatum of Wistar male rats.[17] Seventeen days later, tumor size was measured by magnetic resonance imaging (MRI) using the T2 method. First, we compared Mock and CM21SD groups with the untreated control group. There was no significant difference between these groups. Then, we evaluated the inhibitory effects of miR-21 decoys on tumor growth by comparing LM21D and CM21D with Mock and CM21SD, respectively. Compared with the controls, both CM21D and LM21D significantly decreased the size of the C6 tumor in these animals. CM21D was more efficient than LM21D in suppressing tumor growth (Figures 8A and 8B). This observation is consistent with previous reports showing that circRNAs are more stable than the linear form. According to these premises, CM21D could achieve better results in forthcoming clinical trials.

DISCUSSION

In this study, our *in silico* analysis of 10 available microarray datasets retrieved from the TCGA and GEO and a survey of previous studies indicated that miR-21-5p is highly expressed in GBM. miR-21 exerts tremendous oncogenic effects in cancer cell tumorigenesis by targeting crucial tumor suppressors in diverse cellular signaling pathways, including migration, proliferation, apoptosis, and cell cycle.[6,27] In addition to intracellular oncogenic effects, miR-21 is expressed in the tumor microenvironment and likely transferred into tumor cells by exosomes.[28,29] In line with these premises, the therapeutic strategy based on miR-21 inhibition will be effective and widely applicable because of disarming cancer cells intracellularly and intercellularly.[6]

Moreover, we generated a novel circRNA decoy, CM21D, using the tRNA-splicing mechanism to sequester the oncogenic effects of miR-21 in GBM *in vitro* and *in vivo* models. In addition, the efficiency of CM21D was compared with a linear form, LM21D. Our results revealed that CM21D is a promising therapeutic tool that works more efficiently than LM21D. Here, we observed that inhibition of miR-21 using designed RNA decoys could restore the expression of tumor suppressors such as TIMP3, RECK, PDCD4, HNRNPK, PTEN, TAp63, SMAD7, BCL11B, BAX, CDKN1A, and CDC25A, and decreased the expression of oncogenes, including MMP2, VEGFA, and BCL2.

Previously, in a GBM rat model, we applied LM21D with three perfect binding sites that decreased the tumor volume.[17] Despite inhibiting cancer cell tumorigenesis, linear miR decoys are sensitive to RNase

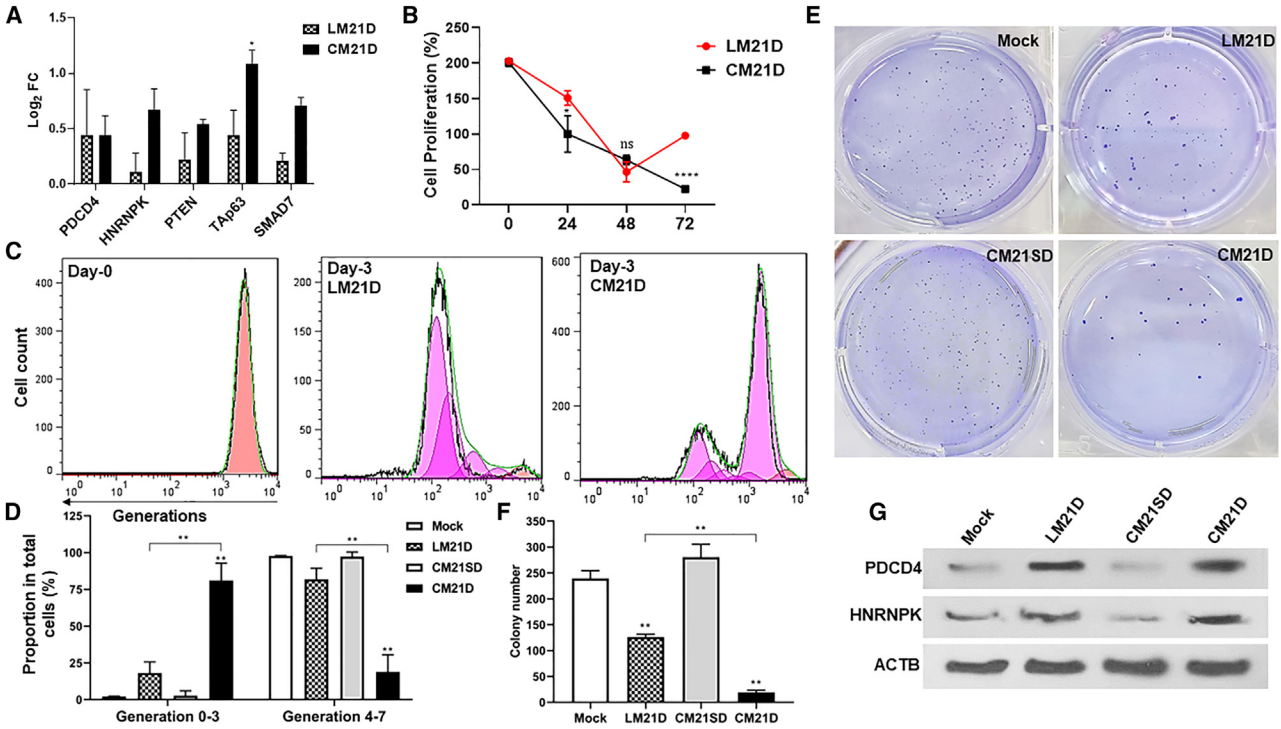

Figure 6. CM21D inhibited cell proliferation more efficiently than LM21D

(A) qRT-PCR was performed to assess the expression level of the genes involved in cell proliferation in U87 cells. (B) MTT assay at different time points (24 h, 48 h, and 72 h) showed that CM21D inhibited cell proliferation in U87 cells more efficiently than LM21D (24 h: $p < 0.05$ and 72 h: $p < 0.001$). (C and D) CSFE assay was performed on U87 cells. The results indicated that CM21D significantly stopped cell proliferation compared to LM21D by observing increased cell number at generations 0–3 and decreased cell number at generations 4–7 ($p < 0.01$). (E and F) Soft agar colony formation assay was performed in U87 cells stably expressing CM21D and LM21D. miR-21 decoys significantly decreased colony formation ($p < 0.01$) and CM21D was more efficient than LM21D ($p < 0.05$) in U87 cells. (G) At the protein level, the expression level of genes involved in cell proliferation was measured by western blotting, and CM21D showed higher efficiency in restoring PDCD4 and HNRNPK expression.

degradation and have shorter half-lives. A class of RNAs generated through back-splicing mechanisms can be circularized, which is more stable than linear forms.[30] These circRNAs have several functions, including miR or protein sponging, transcriptional regulation, mRNA trapping, and translation to produce higher protein amounts.[31,32] Several identified endogenous circRNAs can competitively sponge miR-21 and sequester its downstream effects. *CicrRNA-ACAP2* is an endogenous circRNA that binds to miR-21 and consequently rescues Tiam1 expression in SW480 colon cancer cell lines.[33] Another endogenous circRNA, *circ_0001287*, was overexpressed in a non-small cell lung cancer cell model and increased the expression level of *PTEN* gene by sponging miR-21. Consequently, the invasion, migration, and radioresistance of treated cells were decreased.[11] These naturally occurring circRNAs have been inspired, and artificial synthetic circRNAs established. For the first time, Jost et al.[34] designed an artificial circRNA to sponge miR-122, a critical component in the protein production machinery of the hepatitis C virus. Moreover, Liu et al.[12] generated an artificial circRNA with five bulged binding sites for miR-21 that was more efficient than its linear counterpart in suppressing cell proliferation in gastric cancer. Müller et al.[23] used a synthetic circRNA decoy with four binding sites for miR-21. They delivered it to a lung adenocarcinoma xenograft mouse model using polyethyleneimine-based nanoparticles, significantly inhibiting tumor growth.[23]

Currently, the primary strategy to generate miR decoys involves *in vitro* methods. Although this strategy is efficient and more popular, several drawbacks must be addressed when using this procedure. First, the circularization of larger RNAs with enzymatic ligation is challenging; second, *in vitro* transcription is associated with terminal heterogeneity, which may influence the yield of circularization through enzymatic ligation; and third, to achieve greater RNA purity, it is necessary to digest the circRNA with RNase R and then gel purified, which will decrease the final RNA yield. Finally, co-transfection of RNA and plasmids is difficult and time-consuming and needs to be optimized. Therefore, vector-based strategies have been introduced to facilitate circRNAs production *in vivo*. In this regard, a minigene that circularized after transcription was constructed.[35] Rama et al.[36] established a vector-based protocol using *ALU* sequences to generate a miR decoy with seven binding sites for miR-21 to suppress tumorigenesis in lung cancer cells. Nevertheless, back-splice-imitating constructs are limited in their ability to be delivered using lentiviral particles. The viral constructs are back-spliced in virus-producing cells, interfering with viral transcript packaging.[37] Recently, by applying tRNA splicing

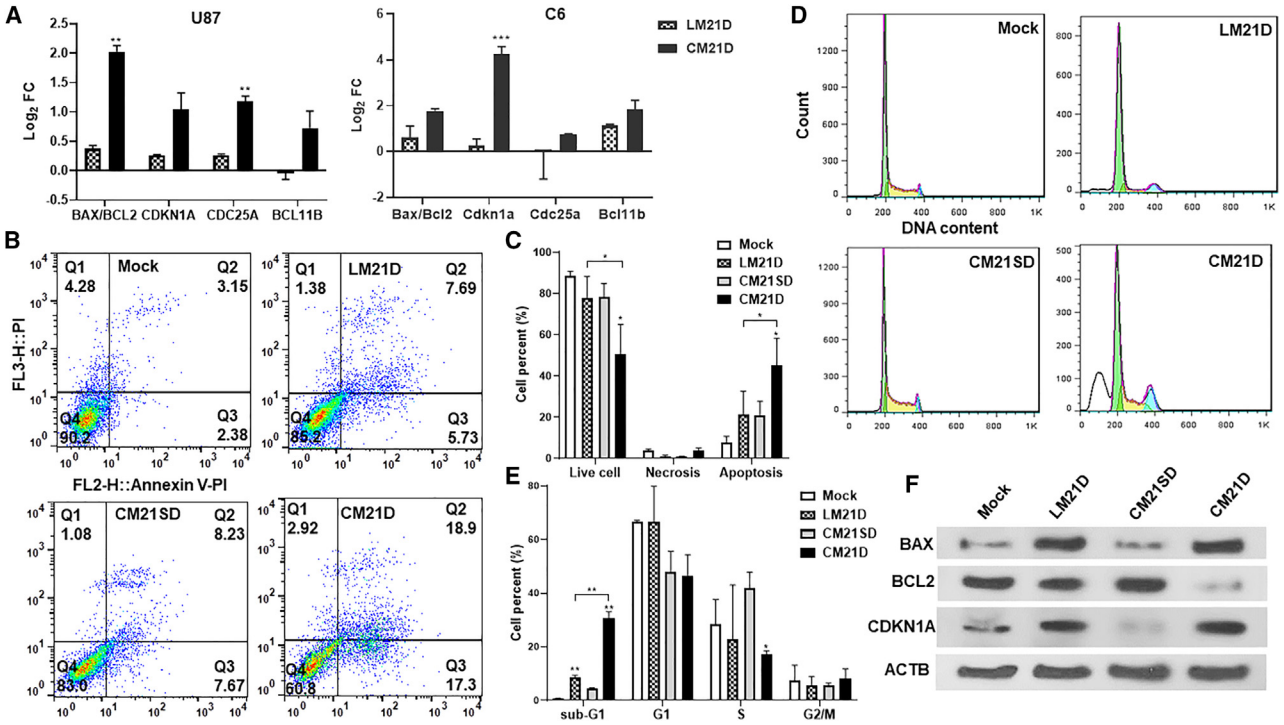

Figure 7. miR-21 decoys impact apoptosis and cell cycle in GBM cells

(A and B) The expression of genes involved in apoptosis and the cell cycle is assessed by qRT-PCR in U87 and C6 cells. (B and C) The apoptosis rate in U87 cells was measured by flow cytometry using Annexin V- propidium iodide (PI) staining. The proportion of live cells decreased in CM21D compared with CM21SD and LM21D ($p < 0.05$). Moreover, CM21D significantly increased the rate of apoptosis compared with CM21SD and LM21D ($p < 0.05$). (D and E) The PI staining showed that LM21D and CM21D significantly increased sub-G1 population cells compared with Mock and CM21SD ($p < 0.01$). In addition, CM21D increased the sub-G1 population more significantly than LM21D ($p < 0.01$). CM21D also decreased the percentage of cells in S-phase as well. (F) The expression of BAX, BCL2 (both involved in apoptosis), and CDKN1A (a cell cycle inhibitor) was measured at the protein level. CM21D was more potent than LM21D in inducing apoptosis and arresting the cell cycle. The ACTB image in Figure 7F is the same as Figure 6G because all the proteins in both figures were analyzed simultaneously.

machinery, an RNA-aptamer production system was established, the Tornado expression system, to manipulate cellular functions. In this study, we used the tRNA-splicing mechanism to bypass previous limitations and generate an artificial circular miR-21 decoy in GBM cells. DFHBI-1T staining confirmed the expression and circularization of our designed circular miR-21 decoy in GBM cell models. This platform can generate circRNAs by subcloning the designed construct between NotI and SacII sites.

TIMP3 and RECK, two critical MMP inhibitors, are direct targets of miR-21 and are downregulated in cancer cells in which miR-21 is upregulated.[38] In this study, we observed that CM21D more efficiently restored the expression levels of TIMP3 and RECK and consequently downregulated MMP2 and VEGFA compared with the linear form at RNA and protein levels. These findings are consistent with previous reports and suggest that CM21D is a promising therapeutic tool for inhibiting tumor cell migration.[39]

Moreover, cell proliferation is a runaway process in cancer cells owing to the inhibition of growth suppressors and prolonged proliferative signaling. Our results indicated that CM21D more efficiently augmented the expression of growth regulators such as PDCD4, HNRNPK, PTEN, TAp63, and SMAD7.[25,26,40,41] As circRNA is more stable than the linear form, our results in the soft agar colony formation assay confirmed the longer inhibitory time of CM21D compared with that of LM21D. Furthermore, cell proliferation is closely correlated with apoptosis and cell cycle regulation. Hence, we estimated BAX/BCL2 ratio at the RNA and protein levels in GBM cells expressing miR-21 decoys. A lower BAX/BCL2 ratio results in increased resistance to apoptosis and an increase in cancer invasion, which correlate with a poor prognosis and vice versa. The increased BAX/BCL2 ratio promotes the release of cytochrome C and consequently activates downstream caspases that trigger apoptosis.[42] Our results indicated that CM21D increased BAX/BCL2 ratio by 4.1-fold compared with the linear form at the protein level. This finding is a significant indicator of an augmented apoptosis rate in cells expressing CM21D. In addition, our results revealed that the expression of genes involved in cell cycle regulation, CDKN1A, CDC25A, and BCL11B, which are direct targets of miR-21, was increased. CDKN1A is a crucial cell cycle inhibitor in the CDKN1A/P53 pathway.[43] Moreover, BCL11B binds to the *MDM2* promoter and inhibits this oncogene, which induces the cell cycle

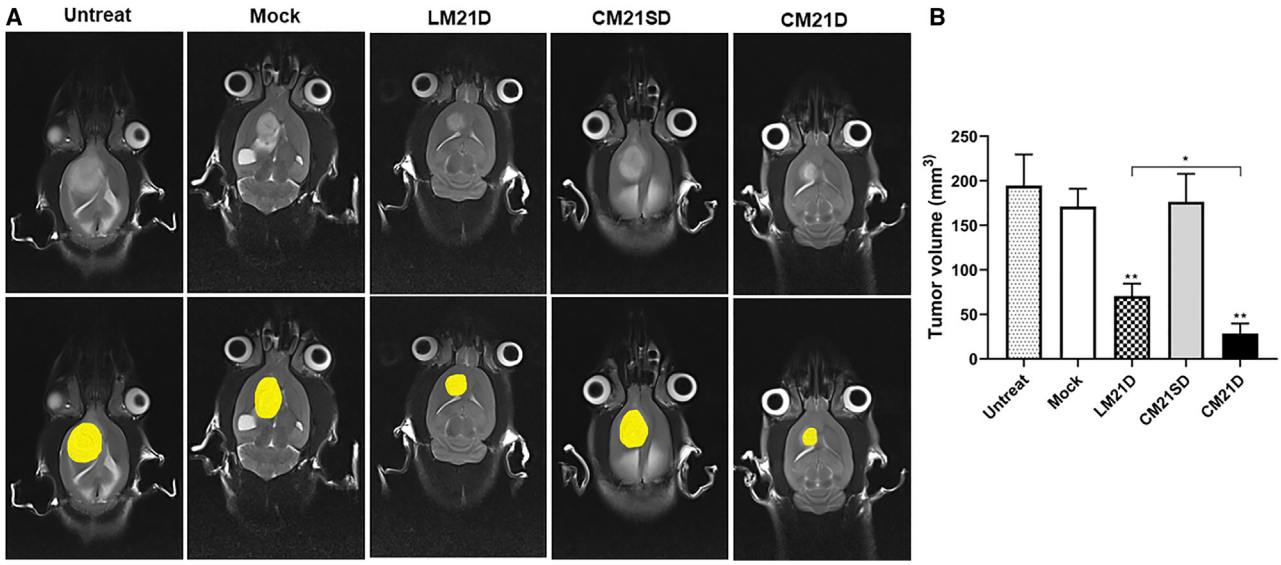

Figure 8. *In vivo* study of miR-21 decoys

(A) C6 cells stably expressing LM21D or CM21D were stereotaxically injected at the caudate putamen striatum (CPu) position in rat brains (1 million cells). MRI evaluated the tumor volume (mm3) in transplanted rats. (B) Both LM21D and CM21D significantly decreased tumor volume compared with Mock and CM21SD, respectively ($p < 0.01$). Moreover, CM21D decreased tumor volume more significantly than LM21D ($p < 0.05$).

in a p53-dependent manner.[44] CDC25A negatively regulates homologous recombination repair by inhibiting cyclin-D1 in cancer cells.[45] Our findings confirmed that the inhibition of miR-21 by designed RNA decoys can arrest the cell cycle by restoring the expression of CDKN1A and BCL11B, which consequently increases in sub-G1 population cells. Moreover, because of the increased levels of CDC25A in cells expressing RNA decoys, these cells probably become more susceptible to radiotherapy, where the inhibition of repair systems is a pivotal step for improved therapy.[46] According to these premises, CM21D was more efficient than the linear form in rescuing the gene expression, inducing apoptosis, and arresting the cell cycle in GBM models.

To confirm that our designed miR-21 decoys had therapeutic effects *in vivo*, we used C6 cells, which are a facsimile of GBM with a relative gene expression pattern.[47] Our findings indicate that CM21D and LM21D could significantly decrease tumor volume, and the repression effect of CM21D was more evident than that of the linear form. This finding confirms the stability and efficiency of CM21D compared with LM21D. Accordingly, CM21D is an intriguing candidate for further analysis in future clinical trials on patients with GBM.

Conclusion

Our results prove that the tRNA-splicing mechanism is a convenient and feasible platform for generating circular miR decoys. Furthermore, CM21D is a potent and efficient therapeutic tool for inhibiting cell migration, proliferation, and cell cycle and inducing apoptosis in GBM cells and probably in other cancers where miR-21 is upregulated. CM21D is a potential RNA-based therapy for simultaneously disarming cancer cells by affecting intracellular signaling pathways and the microenvironment of cancer cells by inhibiting miR-21. The blood-brain barrier is a serious challenge for delivering therapeutic cargo into brain tumor cells. Hence, introducing an applicable procedure, for example, one based on nano- or viral particles, is crucial. Exosomes are nanoparticles that originate from natural cells and can be considered a promising strategy for delivering circRNAs. Our previous report indicated that freshly purified exosomes could successfully deliver a LM21D to GBM cells in a C6-xenograft rat model. However, these exosomes were directly injected together with tumor cells.[17] The current results encouraged the design and execution of further work on the development of CM21D.

MATERIALS AND METHODS

In silico analysis

The GBM dataset was retrieved from TCGA using TCGAbiolinks (RRID: SCR_017683),[48] and nine datasets were downloaded from the GEO database (Table S2). To achieve a reliable intent, all the mentioned GBM datasets with at least one tumor sample and normal were merged using the sva package (RRID: SCR_012836).[49] Furthermore, LIMMA (RRID: SCR_010943) was used for differential expression analysis of retrieved data.[50] Finally, ggplot2 (RRID: SCR_014601) was used to plot all graphs.[51]

Plasmid construction

All PCRs were performed with DNA Polymerase High Fidelity Enzyme (Abbexa; Cat. #abx071010), TA-cloned into pGEM-T Easy Vector Systems (Promega; Cat. #A1360), and validated by performing Sanger sequencing using the Sanger Sequencing 3500 Dx Genetic

Analyzer (Applied Biosystems; Cat. #A27772). The sequences of all the primer sets are listed in Table S3. To construct the circRNA decoy (CM21D/CM21SD), we first amplified the U6 promoter from pSQT1313 (RRID: Addgene_53370) using U6-forward and U6-reverse, which includes 27-nt overhang needs for inducing higher tRNA expression level.[14] Then, it was subcloned into pcDNA 3.1(+) (Invitrogen; Cat. #V79020) between MfeI (Thermo Fisher Scientific; Cat. #ER0752) and HindIII (Thermo Fisher Scientific; Cat. #ER0501) restriction sites (named pU6+27 or Mock). The sequence of CR31905, in which the intron was replaced with CM21D, was synthesized (GeneScript). Subsequently, it was subcloned into HindIII and ApaI (New England Biolabs; Cat. #R0114S) restriction sites (named pCM21D). The bulged miR-21 complementary binding site sequence was 5′-TCAACATCAGAACATAAGCTA-3′. Finally, the sequence of CM21D was replaced with CM21SD; the sequence was 5′- TAATGCGACCACTAAATAACA-3′, using SacII (Thermo Fisher Scientific; Cat. #ER0201) and NotI (New England Biolabs; Cat. #R0189S) restriction enzymes (named pCM21SD). To prevent vector background effects on gene expression, the sequence of linear miR-21 sponges in pTracer-SV40 (Invitrogen; Cat. #V87120) was subcloned into Mock vector between KpnI (New England Biolabs; Cat. #R0142) and ApaI sites (named LM21D). The sequence of all the primers was used in this study, listed in Table S3, and was ordered from GeneScript.

Cell culture, transfection, and generating stable cell line

Human HEK293T (ATCC Cat# CRL-3216, RRID: CVCL_0063) and GBM cell lines, 1321N1 (Sigma-Aldrich Cat# 86030402, RRID: CVCL_0110), A172 (ATCC Cat# CRL-1620, RRID: CVCL_0131), U87 (ATCC Cat# HTB-14, RRID: CVCL_0022), and rat GBM cell line, C6 (ATCC Cat# CCL-107, RRID: CVCL_0194), were cultured in DMEM-F12 (Gibco, Catalog: 12500096) supplemented with 10% FBS (GIBCO, Catalog: A4736401) and 1% penicillin-streptomycin (GIBCO, Catalog:10378016) under optimal growth conditions.

For transfection, the target cell line was seeded in a 24-well plate at a density of 4×10^4 cells/well, 24 h before transfection. At an 80% confluence, 500 μg of the prepared construct was transfected into plated cells using Lipofectamine 3000 Transfection Reagent (Invitrogen; Cat. #L3000008) according to the manufacturer's instructions. Finally, the cells were collected at specific time points for downstream experiments.

To generate stable U87 (stU87) and C6 (stC6) cell lines, 24 h after transfection, the cells were treated with G418 sulfate (BioBasic; Cat. #GDJ958) at 700 μg/mL. The media of the treated cells were exchanged every three days with fresh medium containing G418 sulfate. Genomic DNA (gDNA) and total RNA of stU87 and stC6 cell lines were extracted using the FavorPrep Blood/Cultured Cell Genomic DNA Extraction Mini Kit (Favorgen; Cat. #FABGK 001), and One Step-RNA Reagent (BioBasic; Cat. #BS410A), respectively. The integration of the constructs was confirmed by performing general PCR on gDNAs and qRT-PCR (Applied Biosystems; Cat. #4376357) on total RNA using appropriate primer sets (Table S3).

RNA extraction, cDNA synthesis, and qRT-PCR

Total RNA was extracted, and DNase treatment was performed on the extracted RNA using a DNase I, RNase-free kit (Thermo Fisher Scientific; Cat. #EN0521). The expression of miR-21 was measured via the stem-loop method using SYBR Green reagent (BioFact; Cat. #DQ385).[17] Moreover, the expression of RNA decoys and all genes were measured using specific primer sets (Table S3). 5SrRNA was used as a reference gene for evaluating miR-21 and the RNA decoy expression levels (based on the threshold cycle, ct, and measured using the $2^{-\Delta ct}$ and $\log_2$ ($2^{-\Delta\Delta ct}$) formulas, respectively). *ACTB* and *Gapdh* were used as internal controls in the U87 and C6 cell lines, respectively, to normalize the mRNA expression levels, which were then calculated using the $\log_2$ ($2^{-\Delta\Delta ct}$) formula. StepOne Software (RRID: SCR_014281) was used to analyze the data.

Intracellular staining of circular miR decoy

To visualize the expression of circRNA decoys in U87 and C6 cell lines, 4×10^4 cells/well were seeded in 12-well plates, and 48 h later, the cultured cells were washed with PBS 1×. Cells were then fixed by adding 400 μL of 4% paraformaldehyde (Sigma-Aldrich; Cat. #158127) and incubated at 37 °*C* for 15 min. The cells were then washed three-time with PBS each for 5 min. We obtained 4′,6-Diamidino-2-Phenylindole, Dihydrochloride (DAPI) (Sigma-Aldrich; Cat. #D8417) stock solution (1 mg/mL), and a concentration of 300 nM was used to stain the nuclei of the cells for 3 min. The stained cells were washed with PBS and stained with DFHBI-1T fluorophore (Sigma-Aldrich; Cat. #SML2697), at a concentration of 40 μM, and incubated at 37 °*C* for 30 min. Finally, the prepared slides were photographed using an Olympus IX-53 (RRID: SCR_015801).

Dual luciferase assay

To determine the functionality of the RNA decoys, TIMP3 3′-UTR was amplified and cloned into a psiCHECK^{TM}-2 vector (Promega; Cat. #C8021) between XhoI (Thermo Fisher Scientific; Cat. #ER0691) and NotI (named pTIMP3-UTR).[24] To construct the miR-21 overexpression vector, the precursor sequence of miR-21 was amplified and cloned into the pmR-mCherry vector (Takarabio; Cat. #632542) between EcoRI (Thermo Fisher Scientific; Cat. #ER0521) and BamHI (Thermo Fisher Scientific; Cat. #ER0055) (named pmiR-21). One day before transfection, HEK293T cells were seeded (1.4×10^4 cells/well) in a 48-well plate. Appropriate combinations of constructs were co-transfected into HEK293T cells. After 48 h, the restoration of Renilla's activity was evaluated using the Dual-Luciferase Reporter Assay kit (Promega; Cat. #E1910) according to the manufacturer's protocol.

Wound-healing assay

To assess the migration inhibitory effects of the RNA decoys, U87 and C6 cells were seeded (4×10^4 cells/well) in a 24-well plate with three replications. After 24 h, the constructed plasmids transiently were transfected using Lipofectamine 3000 Transfection Reagent. A 100-μL filter tip was used to scratch the cells 6 h after performing transfection; cell migration was evaluated and photographed under an inverted microscope at 0, 24, and 48 h. The

gap closure percent was estimated using ImageJ software as previously described.[52]

Transwell migration assay

In a sterile environment, stable cell lines were resuspended in a serum-free cell culture medium containing 0.1% BSA (BioBasic; Cat. #AD0023). A total of 1×10^5 cells/500 μL were added on top of a 24 mm filter with an 8-μm pore size (Corning; Cat. #3428). The chambers were then put into the six-well plate containing DMEM-F12 supplemented with 10% FBS. After 24 h, the remaining cells in the top layer were scrubbed with a cotton swab, and the migrated cells on the bottom surface were fixed with 70% ETOH (Merck; Cat. #107017) and stained with 0.2% crystal violet (Sigma-Aldrich; Cat. #C0775).[53] Finally, the number of migrated cells was counted and photographed under an inverted microscope.

MTT assay

One day before transfection, the U87 and C6 cells were seeded (4×10^3 cells/well) in 96-well plates. Three replicates were used for each experiment. Six hours after transfection, the supernatant of transfectants was discarded, and a fresh DMEM-F12 medium supplemented with 10% FBS was added. The MTT assay was performed at 24, 48, and 72 h after transfection using a 5 mg/mL stock solution of 3-(4, 5 methylthiazol-2-yl)-2,5-diphenyl-tetrazolium bromide (10% of total volume added) (Sigma-Aldrich; Cat. #M2003). After 4 h of incubation under optimal growth conditions, the supernatant was discarded, and the formazan crystals were solubilized in 100 μL DMSO (Merck; Cat. #D8418) for 15 min at 37 °C. The color intensity, representing cell proliferation, was measured at 570 nm using an absorbance microplate reader (BioTeck; Cat. #ELx800).

Carboxyfluorescein diacetate succinimidyl ester proliferation assay

U87 and C6 cells were labeled with 1 μL/mL carboxyfluorescein diacetate succinimidyl ester (BioLegend; Cat. #423801) according to the manufacturer's recommendations. The labeled cells were plated at a number of 1.5×10^5 cells/well in a six-well plate. After 16 h, cells were transfected with RNA decoys. The proliferation rate of transfectants was evaluated after 48 h under optimal growth conditions using flow cytometry. The samples were stained with 7-AAD (1 μL/10^6 cells; Biolegend; Cat. #420403) to identify dead cells. Finally, cell proliferation was evaluated using the BD FACSCalibur Flow Cytometry System (RRID: SCR_000401).

Soft agar colony formation assay

The bottom layer of the six-well plate was coated with pre-warmed 2× DMEM-F12 supplemented with 20% FBS and 2% penstrep/streptomycin and diluted with melted 1% agar (BioBasic; Cat. #FB0010) at a ratio of 1:1 and incubated at room temperature for 20 min. The stU87 and stC6 cells in a number of 2.5×10^3 cells/well were resuspended in 2× DMEM-F12 supplemented with 20% FBS and 2% penstrep/streptomycin and diluted with melted 0.7% agarose (BioBasic; Cat. #D0012) at a ratio of 1:1. The mixture was immediately transferred to a coated six-well plate and incubated at optimal growth conditions for 30 days. The cell medium was changed twice a week. Finally, the colons were fixed with 4% paraformaldehyde and stained with 0.005% Crystal Violet. The stained clones were photographed and counted using ImageJ software (RRID: SCR_003070).

Apoptosis assay

U87 and C6 cells were seeded (4×10^4 cells/well) in 24-well plates, and after 16 h, the construct of the RNA decoys were transfected using Lipofectamine 3000 Transfection Reagent. After 48 h, the transfectants were washed twice with PBS 1× and collected with Trypsin-EDTA 0.25% (GIBCO; Cat. #25200056). The collected cells were stained using the Annexin-V-FLUOS Staining Kit (Roche; Cat. #11988549001) and incubated for 15 min at room temperature in the dark. Finally, the apoptosis rate was measured using the FACSCalibur Flow Cytometry System and analyzed using FlowJo v.10 (RRID: SCR_008520).

Cell cycle assay

On a 24-well plate, U87 and C6 cells were seeded at a density of 4×10^4 cells/well, and after 16 h at 80% confluence, the cells were transfected with the construct of the RNA decoys using Lipofectamine 3000 Transfection Reagent. After 48 h, the cells were collected using trypsin-EDTA, washed with PBS 1×, and fixed with ice-cold 70% ETOH. Fixed cells were stained with 20 μg/mL propidium iodide and incubated in the dark at room temperature for 30 min. Finally, the DNA content of the stained cells was evaluated using the FACSCalibur Flow Cytometry System. The results were analyzed using FlowJo v.10 software.

Immunoblotting assay

Total protein was extracted from stable cell lines that expressed expressing RNA decoys using RIPA buffer (Cell Signaling Technology; Cat. #9806) on ice. The concentration of the extracted total protein was measured using the Bradford assay at 490 nm. To separate extracted total proteins, 10% SDS-polyacrylamide gel electrophoresis was used. Proteins were then transferred to a polyvinylidene difluoride membrane (Thermo Fisher Scientific; Cat. #88518) and blocked with 5% BSA at room temperature. Membranes were then incubated with primary antibodies at 4 °C overnight. The specific monoclonal antibodies, used in this study, were as follows: anti-TIMP3, molecular weight: 30 kDa (dilution ratio 1:1,000, Santa Cruz Biotechnology Cat# sc-373839, RRID: AB_11008081), anti-RECK, molecular weight: 110 kDa (dilution ratio 1:1,000, Santa Cruz Biotechnology Cat# sc-373929, RRID: AB_10918105), anti-MMP2, molecular weight: 72 & 63 kDa (dilution ratio 1:1000, Santa Cruz Biotechnology Cat# sc-10736, RRID: AB_2250826), anti-HNRNPK, molecular weight: 65 kDa (dilution ratio 1:100,000, Santa Cruz Biotechnology Cat# sc-28380, RRID: AB_627734), anti-PDCD4, molecular weight: 54 kDa (dilution ratio 1:1,000, Santa Cruz Biotechnology Cat# sc-376430, RRID: AB_11150310), anti-BAX, molecular weight: 23 kDa (dilution ratio 1:1,000, Santa Cruz Biotechnology Cat# sc-7480, RRID:AB_626729), anti-BCL2, molecular weight: 26 kDa (dilution ratio 1:1,000, Santa Cruz Biotechnology Cat# sc-7382, RRID: AB_626736), anti-CDKN1A, molecular weight: 21 kDa (dilution

ratio 1:1,000, Santa Cruz Biotechnology Cat# sc-6246, RRID: AB_628073), and anti-ACTB, molecular weight: 43 kDa (dilution ratio 1:1,000, Santa Cruz Biotechnology Cat# sc-47778, RRID: AB_626632). The membranes were then washed with Tris-buffered saline-Tween solution and exposed to secondary HRP-conjugated mouse anti-rabbit IgG (dilution ratio 1:10,000, Santa Cruz Biotechnology Cat# sc-2357, RRID: AB_628497) and Mouse IgG_κ light chain binding protein (dilution ratio 1:10,000, Santa Cruz Biotechnology Cat# sc-516102, RRID: AB_2687626). Protein bands were visualized using Pierce ECL Western Blotting Substrate (Thermo Fisher Scientific; Cat. #32106) and photographed. Densitometry of the western blot was quantified using ImageJ software.

C6-xenograft rat model

Male Wistar rats (RRID: RGD_12879431) (200–250 g) were purchased from the Production and Research Complex Pasteur Institute of Iran. To generate the GBM xenograft rat model, C6 and stC6 cells expressing Mock, LM21D, CM21SD, and CM21D constructs in a number of 1×10^6 cells in 10 μL PBS were stereotaxically injected at the caudate putamen striatum (2 mm up and right from bregma, at a depth of 4 mm). Each group included three rats. After 17 days, the tumor production for each animal was confirmed by MRI (Siemens 3T Magnetom Skyra MRI scanner; RRID: SCR_020530) with the T2 method, and the volume was measured using ITK-SNAP v3.8.0 (RRID: SCR_002010) for manual segmentation analysis. Animal studies were approved by the Ethics Committees of Tarbiat Modares University (IR.MODARES.REC.1399.170) and the National Institute for Medical Research Development (NIMAD) (IR.NIMAD.REC.1399.272).

Statistical analyses

GraphPad Prism (RRID: SCR_002798) was used to evaluate all quantitative results. The data of all experiments signify an average of two or three autonomous repeats. The statistically substantial changes were quantified with the ordinary ANOVA test and t-test. When the $p < 0.05$, the differences were considered significant.

DATA AND MATERIALS AVAILABILITY

All data generated or analyzed during this study are included in this published article (and its supplementary information files).

SUPPLEMENTAL INFORMATION

Supplemental information can be found online at https://doi.org/10.1016/j.omtn.2023.04.001.

ACKNOWLEDGMENTS

This work was supported by the National Institute for Medical Research Development (NIMAD) (grant numbers 996213, 2020). Also, we thank Niloofar Zarouni for helping us design the graphical pictures.

AUTHOR CONTRIBUTIONS

Conceptualization and design: H.B.; bioinformatics analysis and interpretation of data: H.B. and S.R.; *in vitro* functional analyses and data curation: H.B., M.H.P, and S.J.M.; *in vivo* study: H.B., S.P., and M.H.P.; writing original draft preparation: H.B.; reviewing original draft preparation: M.H.P. and S.J.M.; study advising: M.H.P.; study supervision: S.J.M.

DECLARATION OF INTERESTS

The authors declare that they have no competing interests.

REFERENCES

1. Fabbro-Peray, P., Zouaoui, S., Darlix, A., Fabbro, M., Pallud, J., Rigau, V., Mathieu-Daude, H., Bessaoud, F., Bauchet, F., Riondel, A., et al. (2019). Association of patterns of care, prognostic factors, and use of radiotherapy-temozolomide therapy with survival in patients with newly diagnosed glioblastoma: a French national population-based study. J. Neuro Oncol. *142*, 91–101.
2. Rong, L., Li, N., and Zhang, Z. (2022). Emerging therapies for glioblastoma: current state and future directions. J. Exp. Clin. Cancer Res. *41*, 142.
3. Petrescu, G.E.D., Sabo, A.A., Torsin, L.I., Calin, G.A., and Dragomir, M.P. (2019). MicroRNA based theranostics for brain cancer: basic principles. J. Exp. Clin. Cancer Res. *38*, 231.
4. Rhim, J., Baek, W., Seo, Y., and Kim, J.H. (2022). From molecular mechanisms to therapeutics: understanding MicroRNA-21 in cancer. Cells *11*, 2791.
5. Li, W., Dong, X., He, C., Tan, G., Li, Z., Zhai, B., Feng, J., Jiang, X., Liu, C., Jiang, H., and Sun, X. (2019). LncRNA SNHG1 contributes to sorafenib resistance by activating the Akt pathway and is positively regulated by miR-21 in hepatocellular carcinoma cells. J. Exp. Clin. Cancer Res. *38*, 183.
6. Wang, Y., Malik, S., Suh, H.W., Xiao, Y., Deng, Y., Fan, R., Huttner, A., Bindra, R.S., Singh, V., Saltzman, W.M., and Bahal, R. (2023). Anti-seed PNAs targeting multiple oncomiRs for brain tumor therapy. Sci. Adv. *9*, eabq7459.
7. Jiang, Y., Zhao, J., Li, R., Liu, Y., Zhou, L., Wang, C., Lv, C., Gao, L., and Cui, D. (2022). CircLRFN5 inhibits the progression of glioblastoma via PRRX2/GCH1 mediated ferroptosis. J. Exp. Clin. Cancer Res. *41*, 307.
8. Li, C., Guan, X., Jing, H., Xiao, X., Jin, H., Xiong, J., Ai, S., Wang, Y., Su, T., Sun, G., et al. (2022). Circular RNA circBFAR promotes glioblastoma progression by regulating a miR-548b/FoxM1 axis. Faseb. J. *36*, e22183.
9. Luo, K., Liu, A., Wu, H., Liu, Q., Dai, J., Liu, Y., and Wang, Z. (2022). CircKIF4A promotes glioma growth and temozolomide resistance by accelerating glycolysis. Cell Death Dis. *13*, 740.
10. Wang, Y., Zheng, F., Wang, Z., Lu, J., and Zhang, H. (2020). Circular RNA circSLC7A6 acts as a tumor suppressor in non-small cell lung cancer through abundantly sponging miR-21. Cell Cycle *19*, 2235–2246.
11. Zhang, C.C., Li, Y., Feng, X.Z., and Li, D.B. (2021). Circular RNA circ_0001287 inhibits the proliferation, metastasis, and radiosensitivity of non-small cell lung cancer cells by sponging microRNA miR-21 and up-regulating phosphatase and tensin homolog expression. Bioengineered *12*, 414–425.
12. Liu, X., Abraham, J.M., Cheng, Y., Wang, Z., Wang, Z., Zhang, G., Ashktorab, H., Smoot, D.T., Cole, R.N., Boronina, T.N., et al. (2018). Synthetic circular RNA functions as a miR-21 sponge to suppress gastric carcinoma cell proliferation. Mol. Ther. Nucleic Acids *13*, 312–321.
13. Ebert, M.S., and Sharp, P.A. (2010). MicroRNA sponges: progress and possibilities. RNA *16*, 2043–2050.
14. Schmidt, C.A., Noto, J.J., Filonov, G.S., and Matera, A.G. (2016). A method for expressing and imaging abundant, stable, circular RNAs in vivo using tRNA splicing. Methods Enzymol. *572*, 215–236.
15. Schmidt, C.A., Giusto, J.D., Bao, A., Hopper, A.K., and Matera, A.G. (2019). Molecular determinants of metazoan tricRNA biogenesis. Nucleic Acids Res. *47*, 6452–6465.
16. Nieland, L., van Solinge, T.S., Cheah, P.S., Morsett, L.M., El Khoury, J., Rissman, J.I., Kleinstiver, B.P., Broekman, M.L.D., Breakefield, X.O., and Abels, E.R. (2022). CRISPR-Cas knockout of miR21 reduces glioma growth. Mol. Ther. Oncolytics *25*, 121–136.

17. Monfared, H., Jahangard, Y., Nikkhah, M., Mirnajafi-Zadeh, J., and Mowla, S.J. (2019). Potential therapeutic effects of exosomes packed with a miR-21-sponge construct in a rat model of glioblastoma. Front. Oncol. *9*, 782.

18. Yang, Q., and Wu, G. (2022). CircRNA-001241 mediates sorafenib resistance of hepatocellular carcinoma cells by sponging miR-21-5p and regulating TIMP3 expression. Gastroenterol. Hepatol. *45*, 742–752.

19. Sadeghipour, N., Kumar, S.U., Massoud, T.F., and Paulmurugan, R. (2022). A rationally identified panel of microRNAs targets multiple oncogenic pathways to enhance chemotherapeutic effects in glioblastoma models. Sci. Rep. *12*, 12017.

20. Mo, Y., Zhang, Y., Mo, L., Wan, R., Jiang, M., and Zhang, Q. (2020). The role of miR-21 in nickel nanoparticle-induced MMP-2 and MMP-9 production in mouse primary monocytes: in vitro and in vivo studies. Environ. Pollut. *267*, 115597.

21. Chang, W.T., Lin, Y.W., Huang, P.S., Lin, Y.C., Tseng, S.Y., Chao, T.H., Chen, Z.C., Shih, J.Y., and Hong, C.S. (2022). Deletion of MicroRNA-21 impairs neovascularization following limb ischemia: from bedside to bench. Front. Cardiovasc. Med. *9*, 826478.

22. Yu, L., Lu, J., Xie, H., Ni, J., Chen, S., Zhao, Q., Xie, N., Lu, L., Wang, X., and Li, B. (2022). RELA-Induced MiR-21 exerts oncogenic effects on PDAC via targeting of ARHGAP24. J. Cancer *13*, 2781–2797.

23. Müller, S., Wedler, A., Breuer, J., Glaß, M., Bley, N., Lederer, M., Haase, J., Misiak, C., Fuchs, T., Ottmann, A., et al. (2020). Synthetic circular miR-21 RNA decoys enhance tumor suppressor expression and impair tumor growth in mice. NAR Cancer *2*, zcaa014.

24. Dai, J., Lin, Y., Duan, Y., Li, Z., Zhou, D., Chen, W., Wang, L., and Zhang, Q.Q. (2017). Andrographolide inhibits angiogenesis by inhibiting the mir-21-5p/TIMP3 signaling pathway. Int. J. Biol. Sci. *13*, 660–668.

25. Papagiannakopoulos, T., Shapiro, A., and Kosik, K.S. (2008). MicroRNA-21 targets a network of key tumor-suppressive pathways in glioblastoma cells. Cancer Res. *68*, 8164–8172.

26. Liu, L.H., Fang, C.K., Ge, F.C., Wang, J.N., Zhang, X.B., Luo, R., Zhang, Y., Feng, K.L., Qiu, Z.W., and Zhong, C. (2022). JPHYD inhibits miR-21-5p/smad7-mediated epithelial-mesenchymal transition of hepatocellular carcinoma cells. JAMA Oncol. *2022*, 7823433.

27. Chi, L.H., Cross, R.S.N., Redvers, R.P., Davis, M., Hediyeh-Zadeh, S., Mathivanan, S., Samuel, M., Lucas, E.C., Mouchemore, K., Gregory, P.A., et al. (2022). MicroRNA-21 is immunosuppressive and pro-metastatic via separate mechanisms. Oncogenesis *11*, 38.

28. Nouraee, N., Van Roosbroeck, K., Vasei, M., Semnani, S., Samaei, N.M., Naghshvar, F., Omidi, A.A., Calin, G.A., and Mowla, S.J. (2013). Expression, tissue distribution and function of miR-21 in esophageal squamous cell carcinoma. PLoS One *8*, e73009.

29. Ren, W., Hou, J., Yang, C., Wang, H., Wu, S., Wu, Y., Zhao, X., and Lu, C. (2019). Extracellular vesicles secreted by hypoxia pre-challenged mesenchymal stem cells promote non-small cell lung cancer cell growth and mobility as well as macrophage M2 polarization via miR-21-5p delivery. J. Exp. Clin. Cancer Res. *38*, 62.

30. Zeng, Z., Xia, L., Fan, S., Zheng, J., Qin, J., Fan, X., Liu, Y., Tao, J., Liu, Y., Li, K., et al. (2021). Circular RNA CircMAP3K5 acts as a MicroRNA-22-3p sponge to promote resolution of intimal hyperplasia via TET2-mediated smooth muscle cell differentiation. Circulation *143*, 354–371.

31. Tan, K.E., and Lim, Y.Y. (2021). Viruses join the circular RNA world. FEBS J. *288*, 4488–4502.

32. Chen, R., Wang, S.K., Belk, J.A., Amaya, L., Li, Z., Cardenas, A., Abe, B.T., Chen, C.K., Wender, P.A., and Chang, H.Y. (2023). Engineering circular RNA for enhanced protein production. Nat. Biotechnol. *41*, 293.

33. He, J.H., Li, Y.G., Han, Z.P., Zhou, J.B., Chen, W.M., Lv, Y.B., He, M.L., Zuo, J.D., and Zheng, L. (2018). The CircRNA-ACAP2/hsa-miR-21-5p/Tiam1 regulatory feedback circuit affects the proliferation, migration, and invasion of colon cancer SW480 cells. Cell. Physiol. Biochem. *49*, 1539–1550.

34. Jost, I., Shalamova, L.A., Gerresheim, G.K., Niepmann, M., Bindereif, A., and Rossbach, O. (2018). Functional sequestration of microRNA-122 from Hepatitis C Virus by circular RNA sponges. RNA Biol. *15*, 1032–1039.

35. Obi, P., and Chen, Y.G. (2021). The design and synthesis of circular RNAs. Methods *196*, 85–103.

36. Rama, A.R., Quiñonero, F., Mesas, C., Melguizo, C., and Prados, J. (2022). Synthetic circular miR-21 sponge as tool for lung cancer treatment. Int. J. Mol. Sci. *23*, 2963.

37. Mecozzi, N., Nenci, A., Vera, O., Bok, I., Falzone, A., DeNicola, G.M., and Karreth, F.A. (2022). Genetic tools for the stable overexpression of circular RNAs. RNA Biol. *19*, 353–363.

38. Bai, X., and Bian, Z. (2022). MicroRNA-21 is a versatile regulator and potential treatment target in central nervous system disorders. Front. Mol. Neurosci. *15*, 842288.

39. Shen, K.H., Hung, J.H., Liao, Y.C., Tsai, S.T., Wu, M.J., and Chen, P.S. (2020). Sinomenine inhibits migration and invasion of human lung cancer cell through downregulating expression of miR-21 and MMPs. Int. J. Mol. Sci. *21*, 3080.

40. Chen, M., Medarova, Z., and Moore, A. (2021). Role of microRNAs in glioblastoma. Oncotarget *12*, 1707–1723.

41. Sabry, R., Williams, M., Werry, N., LaMarre, J., and Favetta, L.A. (2022). BPA decreases PDCD4 in bovine granulosa cells independently of miR-21 inhibition. Int. J. Mol. Sci. *23*, 8276.

42. Shin, J.W., Kwon, S.B., Bak, Y., Lee, S.K., and Yoon, D.Y. (2018). BCI induces apoptosis via generation of reactive oxygen species and activation of intrinsic mitochondrial pathway in H1299 lung cancer cells. Sci. China Life Sci. *61*, 1243–1253.

43. Dabiri, Y., Abu El Maaty, M.A., Chan, H.Y., Wölker, J., Ott, I., Wölfl, S., and Cheng, X. (2019). p53-Dependent anti-proliferative and pro-apoptotic effects of a gold(I) N-heterocyclic carbene (NHC) complex in colorectal cancer cells. Front. Oncol. *9*, 438.

44. Zhang, L., Yu, L., Liu, Y., Wang, S., Hou, Z., and Zhou, J. (2021). miR-21-5p promotes cell proliferation by targeting BCL11B in Thp-1 cells. Oncol. Lett. *21*, 119.

45. Hu, B., Wang, X., Hu, S., Ying, X., Wang, P., Zhang, X., Wang, J., Wang, H., and Wang, Y. (2017). miR-21-mediated radioresistance occurs via promoting repair of DNA double strand breaks. J. Biol. Chem. *292*, 3531–3540.

46. Kang, T., Wei, Y., Honaker, Y., Yamaguchi, H., Appella, E., Hung, M.C., and Piwnica-Worms, H. (2008). GSK-3 beta targets Cdc25A for ubiquitin-mediated proteolysis, and GSK-3 beta inactivation correlates with Cdc25A overproduction in human cancers. Cancer Cell *13*, 36–47.

47. Pagilla, S., Anagani Kanaka Durga, B., Vodnala, S., Kamutam, R., Mudiraj, A., Phanithi, P.B., and Chetti, P. (2022). Identification of novel quinazolinone hybrids as cytotoxic agents against C6 glioma cell lines. J. Chin. Chem. Soc. *69*, 968–978.

48. Colaprico, A., Silva, T.C., Olsen, C., Garofano, L., Cava, C., Garolini, D., Sabedot, T.S., Malta, T.M., Pagnotta, S.M., Castiglioni, I., et al. (2016). TCGAbiolinks: an R/Bioconductor package for integrative analysis of TCGA data. Nucleic Acids Res. *44*, e71.

49. Leek, J.T., Johnson, W.E., Parker, H.S., Jaffe, A.E., and Storey, J.D. (2012). The sva package for removing batch effects and other unwanted variation in high-throughput experiments. Bioinformatics *28*, 882–883.

50. Ritchie, M.E., Phipson, B., Wu, D., Hu, Y., Law, C.W., Shi, W., and Smyth, G.K. (2015). Limma powers differential expression analyses for RNA-sequencing and microarray studies. Nucleic Acids Res. *43*, e47.

51. Wickham, H. (2016). ggplot2: Elegant Graphics for Data Analysis (New York: Springer, Verlag).

52. Suarez-Arnedo, A., Torres Figueroa, F., Clavijo, C., Arbeláez, P., Cruz, J.C., and Muñoz-Camargo, C. (2020). An image J plugin for the high throughput image analysis of in vitro scratch wound healing assays. PLoS One *15*, e0232565.

53. Justus, C.R., Leffler, N., Ruiz-Echevarria, M., and Yang, L.V. (2014). In vitro cell migration and invasion assays. JoVE *88*, e51046.